

Substitutional Ta-doping in Y_2O_3 semiconductor by sol-gel synthesis: experimental and theoretical studies

Diego Richard^{1,4,5} , Mario Rentería²  and Artur Wilson Carbonari³ 

¹Centro NanoMat/DETEMA, Facultad de Química, Universidad de la República (UdelaR), CC 1157, Montevideo, Uruguay

²Departamento de Física and Instituto de Física La Plata (IFLP, CONICET), Facultad de Ciencias Exactas, Universidad Nacional de La Plata, CC 67, (1900) La Plata, Argentina

³Instituto de Pesquisas Energéticas e Nucleares, Universidade de São Paulo, 05508-000 São Paulo, SP, Brazil

E-mail: richard@fisica.unlp.edu.ar, reneria@fisica.unlp.edu.ar and carbonar@ipen.br

Received 13 March 2017, revised 18 June 2017

Accepted for publication 20 June 2017

Published 24 July 2017



CrossMark

Abstract

The Pechini sol-gel method has been employed for the synthesis of pure and ($^{181}\text{Hf} \rightarrow$) ^{181}Ta -doped Y_2O_3 nanopowders. We performed a structural characterization from the micro to the subnanoscopic scale by means of scanning electron microscopy, energy dispersive x-ray spectroscopy, x-ray diffraction, and time-differential perturbed γ - γ angular correlation (PAC) spectroscopy. The results show the formation of the cubic *bixbyite* structure after a thermal treatment at 1473 K. For the synthesized ^{181}Ta -doped Y_2O_3 , the PAC experiments demonstrate that the impurities are mainly located at both substitutional cationic sites of the *bixbyite* structure. The experimental investigation was complemented by performing first-principles electronic structure calculations for Ta atoms localized at the two cationic sites of the Y_2O_3 semiconductor structure, which allow the study of the structural and electronic modifications induced in the host system when the impurities are introduced. These calculations confirm that the measured electric-field gradients for the synthesized ^{181}Ta -doped Y_2O_3 correspond to double-ionized impurities located at substitutional defect-free cationic sites of the *bixbyite* host structure and indicate the site occupancy preference for $^{181}\text{Hf}(\rightarrow^{181}\text{Ta})$ doping. The behaviour of the site preference of ^{181}Ta impurities with temperature is also discussed. In addition to an extensive structural and electronic characterization of pure and Ta-doped Y_2O_3 semiconductor, our results demonstrate that the Pechini sol-gel process is an affordable and effective way to successfully synthesize these PAC substitutional doped samples.

Keywords: impurities in semiconductors, oxide materials, sol-gel processes, hyperfine interactions, computer simulations, perturbed angular correlations

(Some figures may appear in colour only in the online journal)

1. Introduction

The study of doped semiconductor oxides has grown in the past years due to their many potential technological applications in current highly relevant topics, such as spintronics [1, 2], gas sensors [3–7], photocatalysis [8, 9] or fuel cells for renewable energies [10]. In this sense, the characterization and modelling of properties related to the inclusion of

⁴ On leave from Departamento de Física and Instituto de Física La Plata (IFLP, CONICET), Facultad de Ciencias Exactas, Universidad Nacional de La Plata, Argentina.

⁵ Author to whom any correspondence should be addressed.

impurities in an oxide nowadays are of an important and increasing interest. Among the preparation methods for this type of doped system, the synthesis by a wide variety of sol-gel processing methods has gained attention (see, for example, [11–15]).

A possible way to study doped systems at the subnanoscopic level is by means of time-differential perturbed γ - γ angular correlation (PAC) spectroscopy, which is based on the interaction of the nuclear moments of a probe nucleus with the extra-nuclear hyperfine fields. PAC is a hyperfine technique that measures the angular correlation of two successive γ -rays emitted during a nuclear decay cascade. Among its capabilities, it allows the determination of the electric-field-gradient (EFG) tensor at a probe-nucleus, quantity which is an observable with highly localized sensitivity due to its $1/r^3$ dependence, r being the distance between the nucleus and the electric charges that originate the EFG [16]. Regarding doped semiconductor oxides, by using the PAC technique it is possible to determine the EFG tensor at the site of a probe atom, which is usually an extremely diluted impurity in the system under study [17, 18]. Hence, this technique is a powerful tool that provides an access to the smallest atomic scale. In particular, its strength lies in the fact that it focuses on the site where the impurity probe atom is located, even if the impurities are extremely diluted. Since the probe is introduced in the host matrix, through this experimental technique we can ‘observe’ the resulting structure from a very distinctive observation point. Moreover, if we complement PAC spectroscopy results with those obtained from other experimental or theoretical methods, we can relate the subnanoscopic structure to the electronic properties that arise after the inclusion of impurities.

As mentioned above, the PAC technique requires the use of radioactive probe nuclei adequately introduced into the host lattice. In this respect, there are different methods to prepare samples that are suitable for their study with PAC spectroscopy. For example, for the most common PAC probe ($^{111}\text{In} \rightarrow ^{111}\text{Cd}$), thermal diffusion [19, 20] and ion implantation [20–24] are frequently used as doping methods, while for the probe ($^{181}\text{Hf} \rightarrow ^{181}\text{Ta}$), ion implantation is a very effective mechanism to prepare the doped oxides [25]. However, these preparation methods, even if all the involved facilities are available at the laboratory, constrain *a priori* the number and the kind of systems accessible to the PAC technique. This is true, specially, for the thermal diffusion method since in many compounds the diffused probe-atom cannot substitute the desired native atoms due, e.g., to chemical reasons. Ion implantation of radioactive isotopes, besides its high cost, is highly efficient in almost all kinds of host systems, being the handicap of this method the difficulty to achieve large doping deepness and high doping rates, and the radiation damage it produces. For these reasons, in order to extend the useful range of the PAC spectroscopy, alternative and low-cost ways to prepare samples have been investigated mainly in the last decade. Among them, we can include those based in solid-state reactions between oxides [26, 27] or the chemical precipitation method [28]. These alternative methods have shown their capability to

successfully introduce the ^{181}Ta probe nuclei in a host matrix, nevertheless, the corresponding PAC experiments usually need additional supporting evidence to reach a complete interpretation of the complex spectra they give. Information of this kind includes parallel control experiments, additional data obtained from compounds with the same crystal structure, or an accurate theoretical prediction for the hyperfine properties [27, 29–31]. Considering all these facts, a current challenge is to find an affordable and effective way to perform the PAC probe doping of host structures. In the best scenario, that doping method should allow us to obtain clean PAC spectra, and the measured hyperfine interactions should allow us to draw a model of the system under study.

In the work reported in this paper, we present a study of the Pechini sol-gel (PSG) method as a way to prepare PAC doped samples. To this purpose, we considered the original sol-gel route proposed by Pechini [32]. In particular, by using this method we will analyse the case of Tantalum-doped Y_2O_3 . Yttria has been extensively studied due to its potential application in a wide range of technological devices, which includes corrosion protective coatings [33], transparent windows [34–36] and lasers [37], among many other applications. Y_2O_3 naturally crystallizes in the cubic *bixbyite*-type structure (C-type sesquioxide, figure 1(a)), which is characterized by two crystallographic cationic sites corresponding to the Wyckoff positions $24d$ with non-centrosymmetric C_2 symmetry, and $8b$ with centrosymmetric C_{3i} [38]. These two non-equivalent sites, hereafter called C and D, respectively, are both coordinated with 6 nearest oxygen neighbours (ONN). The D site is axially symmetric and site C is highly asymmetric, and their relative abundance is $f_C:f_D = 3:1$ [38] (see figures 1(b) and (c)).

In the last decade, different sol-gel routes for synthesizing pure Y_2O_3 have been studied in detail [39–42], showing that these kinds of methods are a rapid and an easy way for preparing this oxide. On the other hand, PAC experiments using the ($^{111}\text{In} \rightarrow ^{111}\text{Cd}$) probe in samples prepared by the PSG method were recently reported. In this respect, two kind of samples were investigated: those prepared by the PSG method followed by the thermal diffusion process of the PAC probe [14, 43], and those in which the radioactive probe was incorporated during the PSG preparation of the oxide [44, 45]. In the present paper, we will extend these investigations to study the case of the semiconductor oxide Y_2O_3 doped with the probe ($^{181}\text{Hf} \rightarrow ^{181}\text{Ta}$). To our knowledge, this is the first time where the sol-gel processing is considered for synthesizing PAC samples with this probe. Therefore, in what follows we present a study of the effectiveness and efficiency of the PSG method to synthesize pure and Ta-doped Y_2O_3 . To this purpose, we used scanning electron microscopy (SEM), energy dispersive x-ray spectroscopy (EDS), x-ray diffraction (XRD), and PAC spectroscopy. These techniques allow the characterization of the oxides at three different scales, the micro, the crystal, and the subnanoscopic structures. The existence of previous EFG measurements in the Y_2O_3 : ^{181}Ta sample prepared by implantation of ^{181}Hf ions [25] gives an ideal frame to evaluate the sol-gel processing. Finally, in order to obtain a complete study of the hyperfine

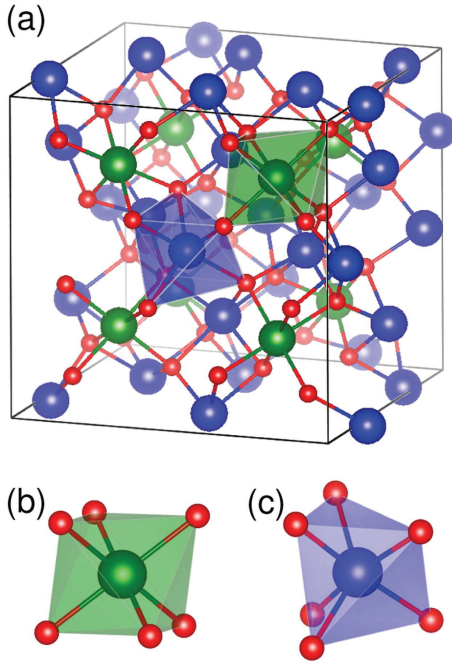


Figure 1. (a) Y_2O_3 bixbyite crystal structure. The large green and blue spheres represent the cationic sites D and C, respectively, and the small red spheres stand for oxygen atoms. (b), (c) Y coordination with its nearest oxygen neighbours (ONNs) at sites D and C, respectively. The upper and lower polyhedra in (a) show these ONN octahedral arrangements (for interpretation of the colour references in this figure legend, the reader is referred to the online version of this article).

properties in these systems, we present first-principles predictions of the EFG at Ta impurities localized at both defect-free cationic sites of the host oxide. For this purpose, we used the augmented plane waves plus local orbitals (APW+lo) method, which is based on density functional theory (DFT) [46]. With this approach, we analysed the role of the impurities in the structural and electronic properties of the doped system, and how the EFG depends on the local structure and the impurity ionization state. The combination of experiment and theory enabled us to obtain a more complete description of the hyperfine properties observed through the PAC technique in the $(^{181}\text{Hf} \rightarrow ^{181}\text{Ta})$ -doped sample prepared by the PSG method.

This paper is organized as follows. In section 2 we briefly describe the PAC technique according to the purposes of our investigation and we describe the sample preparation. In section 3 we present and discuss the experimental results, we briefly outline the way we applied the APW+lo approach and we present and discuss the theoretical predictions of this method. Finally, in section 4 we present our conclusions.

2. Experimental details

2.1. The PAC technique

During a PAC experiment it is determined the perturbation caused by the extra-nuclear fields on the correlation between the emission directions of two successive γ -radiations emitted during the decay of a radioactive probe nucleus. When the probe is surrounded by a charge distribution with non cubic symmetry, an EFG is generated at its site, which can be measured through its interaction with the nuclear quadrupole moment Q of the intermediate nuclear level of the probe's γ - γ cascade [16].

In order to perform the PAC experiments presented in this paper, we employed the probe nucleus ^{181}Ta . We made use of the 133–482 keV γ - γ decay cascade produced after the β^- nuclear decay of the ^{181}Hf isotope, which has a half-life of 42.39 days. The PAC experiments were performed using four lutetium oxyorthosilicate scintillation crystal detectors in a coplanar arrangement at 90° angle to each other [47]. The PAC experimental function, $R(t)$, is derived from the simultaneously measured coincidence spectra, for the detectors positioned at 180° and 90° . The measured $R(t)$ spectra were analysed with the usual models for multiple site nuclear-electric-quadrupole interactions, as done in previous experiments for $(^{181}\text{Hf} \rightarrow ^{181}\text{Ta})$ -doped commercial Y_2O_3 powder prepared by ion implantation [25]. To this purpose, we considered a perturbation factor valid for static nuclear-electric-quadrupole interactions, polycrystalline samples, and spin $I = 5/2+$ of the intermediate nuclear level:

$$R(t) = A_{22}^{\text{exp}} G_{22}(t) = A_{22}^{\text{exp}} \sum_i f_i \left[S_{20,i} + \sum_{n=1}^3 S_{2n,i0} \times \cos(\omega_{n,i}t) \exp(-\delta_i \omega_{n,i}t) \right], \quad (1)$$

where A_{22}^{exp} is the effective anisotropy of the γ - γ cascade, and $G_{22}(t)$ is the perturbation factor. f_i is the fraction of nuclei that experiences a given perturbation. The interaction frequencies ω_n are related to the nuclear-quadrupole frequency $\omega_Q = eQV_{zz}/40\hbar$ by $\omega_n = g_n(\eta)\omega_Q$, where Q is the nuclear-quadrupole moment of the $5/2+$ state of the probe ^{181}Ta . The g_n and S_{2n} coefficients are known functions of the asymmetry parameter $\eta = (V_{xx} - V_{yy})/V_{zz}$, with V_{ii} the principal EFG tensor components ordered following the convention $|V_{xx}| < |V_{yy}| < |V_{zz}|$. Finally, δ is the relative width of a Lorentzian frequency distribution around ω_n . The exponential functions stand for the 'static' damping of the spectra due to the slightly different static (*time-independent*) EFGs that the probes located in equivalent crystal sites observe because of the different distortions in their far surroundings.

2.2. Sample preparation

Pure Y_2O_3 samples were prepared using the PSG method [32]. The starting materials were Y_2O_3 powder (Aldrich), and Y and Hf metal powders (Alfa products), each one with purity better than 99.9%. In addition, we made use of different reagents of analytical grade, which were used without further purification. In order to prepare 500 mg of Y_2O_3 , the

corresponding stoichiometric amount of yttrium metal was dissolved in hydrochloric acid diluted in deionized water. The resulting solution was mixed with citric acid and a few drops of ethylene glycol. This mixture was stirred and heated in an open flask at about 400 K to promote the polymerization, until the gel formation. This precursor gel was maintained under heating until the excess water had substantially evaporated, and then it was calcined for 12 h at 723 K to form the oxide. The resulting powder was pressed into a pellet and thermally treated again for 1 h at 523 K and 12 h at 1473 K. During this annealing procedure, the furnace heating rates were 5 K min^{-1} and 3 K min^{-1} to reach the 523 and 1473 K temperature steps, respectively. After preparation, a piece of the pellet was characterized by SEM, EDS and XRD. In order to compare the results obtained for the sample synthesized by the PSG method, we also prepared a pellet of commercial Y_2O_3 powder, following the same thermal treatment than that mentioned above for the sol-gel powder pellet.

To synthesize the radioactive Ta-doped sample, $\text{Y}_2\text{O}_3\text{:}^{181}\text{Ta}$, we first irradiated 0.2 mg of Hf metal with thermal neutrons at the IEA-R1 research reactor at IPEN for about 60 h. Then, it was dissolved in a drop of hydrofluoric acid, and the resulting $^{181}\text{HfF}_4$ was added to the preparation during the polymerization stage described above. The final impurity concentration of the resulting $^{181}\text{Hf}(\rightarrow^{181}\text{Ta})$ -doped sample was below 0.1 at% of Y (activity below $100 \mu\text{Ci}$). This sample was studied by PAC spectroscopy, after the same pelletization and annealing process as the one detailed for the pure Y_2O_3 .

3. Results and discussion

3.1. Experimental results

3.1.1. Pure Y_2O_3 . In figures 2(a) and (b) we present the SEM micrographs for the Y_2O_3 pellets prepared by the PSG method and from the commercial powder. These images show that both powders are highly agglomerated. The pellets are composed of nano-sized particles, which present sizes that start ranging from about 200 nm, with a mean size of about 400 nm. A distinctive feature is that the PSG sample presents spherical micropores (of about 400 nm diameter), which give to the pellet a foamy aspect at this scale. These micropores are attributed to the combustion of the organics used during the synthesis. The EDS measurements of figure 2(c) show the same contribution of the Y-L and O-K peaks to the x-ray emission spectra in both samples. The Au peaks in those spectra are due to Au coating of the samples, and the minor C peaks result from the carbon adhesive tape used to mount the samples to the SEM stub. The obtained EDS spectra suggest that synthesized PSG sample has the same relative abundance of Y and O than the commercial sesquioxide.

In figure 3 we present the XRD measurements. The diffraction patterns confirm the presence of the cubic *bixbyite* structure (space group *Ia3*) as single phase in both samples. From the analysis by Rietveld refinement we obtained the values for the lattice parameter a and the size of the crystallite

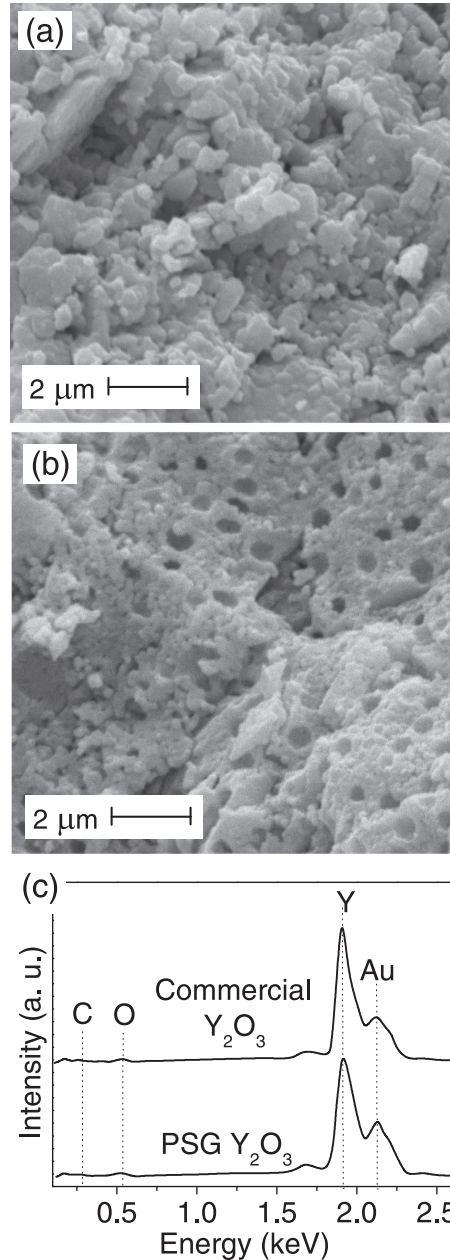


Figure 2. SEM images of (a) commercial and (b) PSG Y_2O_3 samples. In (c), EDS spectra of both samples are shown.

D [48]. For the sample prepared by the PSG method the parameters were determined as $a = 1.06260(2) \text{ nm}$ and $D = 177(2) \text{ nm}$, whereas for that coming from the commercial powder these parameters were found to be $a = 1.06249(4) \text{ nm}$ and $D = 64.5(5) \text{ nm}$. The measurements of the lattice parameter are in good agreement with that corresponding to yttria single crystal ($a = 1.05981(7) \text{ nm}$) [38]. Also, the observed morphology of the PSG sample, with the presence of micropores, is similar to that previously observed for Y_2O_3 powders synthesized by other sol-gel routes that use citric acid as chelating agent [39, 49, 50]. Therefore, although the micro structural morphology of both samples is different, we

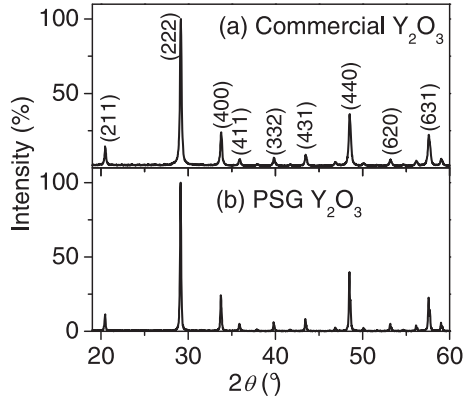


Figure 3. XRD diffraction patterns of (a) commercial and (b) PSG Y_2O_3 samples. All diffraction peaks are indexed as cubic *bixbyite* Y_2O_3 .

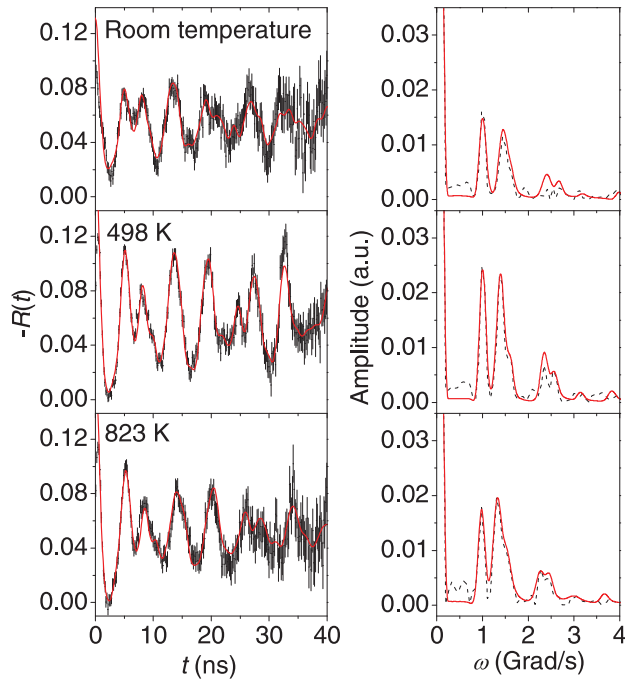


Figure 4. $R(t)$ spectra for Y_2O_3 : ^{181}Ta PSG sample (left) and their Fourier transformed spectra (right) taken at representative measuring temperatures.

showed that the used sol-gel processing method could successfully synthesize cubic Y_2O_3 .

3.1.2. PAC spectra in Y_2O_3 : ^{181}Ta . In figure 4 we present three representative $R(t)$ spectra for the Y_2O_3 : ^{181}Ta PSG sample, and their corresponding Fourier transformed spectra measured at different temperatures T in the range 273–923 K. The solid lines in the PAC spectra are the best least-squares fits of equation (1) to the experimental data. The solid lines in the Fourier spectra are the Fourier transformation of the $R(t)$ fits. Three hyperfine interactions were necessary to account for the experimental spectra. These interactions are very well-defined, being $\delta < 5\%$ in all cases. Figure 5 shows the fitted

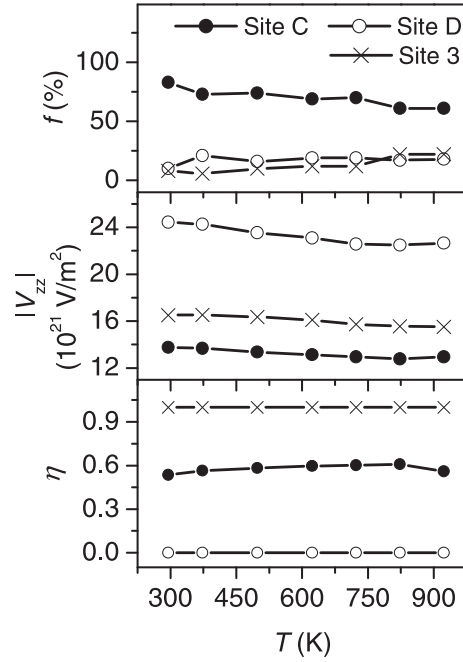


Figure 5. Temperature dependence of the hyperfine parameters for Y_2O_3 : ^{181}Ta PSG sample.

population factor f_i and the $|V_{zz}|$ and η parameters as a function of T (we used $Q = 2.35(6)$ b [51] to obtain $|V_{zz}|$ from the nuclear quadrupole frequencies ω_Q). Two of the measured hyperfine interactions were associated to the ^{181}Ta probes located at substitutional cationic sites C and D of the cubic *bixbyite* structure. We tentatively assigned these hyperfine interactions considering their values of f_i and asymmetry parameter η : the most populated interaction with $\eta \approx 0.5$ corresponds to probes located at the highly asymmetric site C, and the interaction with $\eta \approx 0$ corresponds to impurities located at the axially symmetric site D. According to this interaction assignment, the $f_C:f_D$ ratio ranges from 8 to 3.4 within the measuring temperature interval. At $T = 923$ K this ratio is close to 3, which corresponds to the case of both cationic sites occupied by the ^{181}Ta probe with equal probability. In addition, we observe that $|V_{zz}|$ slightly decreases with increasing T (see figure 5), which is a common behaviour for the case of substitutional PAC probes (see, for example, [52]). These two interactions contribute in 80% or more to the total $R(t)$ spectrum, depending on T . At room temperature, they are characterized by the parameters $|V_{zz}^C| = 13.77(6) \times 10^{21} \text{ V m}^{-2}$, $\eta^C = 0.535(7)$, $|V_{zz}^D| = 24.4(1) \times 10^{21} \text{ V m}^{-2}$, and $\eta^D = 0$ (this last parameter was kept fixed during the fitting procedure). We found that our results are in very good agreement with those previously obtained in $^{181}\text{Hf}(\rightarrow^{181}\text{Ta})$ -implanted Y_2O_3 , where $|V_{zz}^C| = 13.06(3) \times 10^{21} \text{ V m}^{-2}$, $\eta^C = 0.536(4)$, $|V_{zz}^D| = 22.86(7) \times 10^{21} \text{ V m}^{-2}$, and $\eta^D = 0.04(4)$ [25]. The presence of the third interaction in our measurements is associated to the location of ^{181}Ta in an additional probe specific complex. This is suggested by the nearly continuous values of its $|V_{zz}|$ and η parameters, and the increasing of f_3 with increasing T , in a reversible way (see

figure 5). Hence, considering this information, our assumption of ^{181}Ta nuclei mainly located at cationic sites of the *bixbyite* structure is well justified. This result would confirm that the PSG process is an effective method to synthesize also the PAC sample with the probes located at free-of-defect cationic sites of the host structure.

3.2. Computational approach

3.2.1. Method of calculation. We used the WIEN2k implementation [46] of the APW+lo method to perform self-consistent electronic structure calculations from first-principles to study the structural and electronic properties that appear when Y_2O_3 is doped with Ta. To this purpose, we considered the 40-atom *bixbyite* unit cell and we replaced one Y atom belonging to site C or D by a Ta atom. We called the resulting systems $\text{Y}_2\text{O}_3:\text{Ta}(\text{C})$ and $\text{Y}_2\text{O}_3:\text{Ta}(\text{D})$, respectively. The resultant impurity cationic concentration is 1:16. The exchange and correlation energy was treated considering the local density approximation (LDA) [53] and the Wu and Cohen parameterization of the generalized gradient approximation (WCGGA) [54]. We used muffin-tin radii (R_{MT}) of 1.0 Å for Y and Ta atoms, and 0.9 Å for O atoms, and a value of 7 for the RK_{max} parameter, which determines the number of the basis functions. The integration in the reciprocal space was performed using the tetrahedron method, taking up to 100 k points in the Brillouin zone. The validity of the choice of these parameters was checked by performing additional calculations for other values of R_{MT} , RK_{max} , and the k -point sampling.

We used the APW+lo method to calculate the density of electronic states (DOS) of the pure and Ta-doped Y_2O_3 systems, as well as the structural modifications induced by the presence of the impurity. To do this, we started using the cell with its lattice parameter fixed at the experimental value ($a = 1.05981$ nm). This initial structure was called *unrelaxed structure*. The forces on the atoms were calculated self-consistently, and the atoms were displaced until the forces were below a tolerance value of $0.025 \text{ eV } \text{Å}^{-1}$. The resulting structure after this procedure was called *relaxed structure*. In each step of the self-consistent calculation, we determined the diagonal elements of the EFG tensor at the Ta site directly from the $V_{2\text{M}}$ harmonic coefficients of the potential [55, 56].

Since the Ta^{5+} atom is a nominal double donor impurity in $\text{Y}_2^{3+}\text{O}_3^{2-}$, we expect that it will introduce donor-like states in the band gap of the semiconductor's DOS. Therefore, to treat the possible ionization states of the impurity, we removed none, one, or two electrons from the unit cell, and compensated the positive charge with a negative homogeneous charge background.

The described first-principles procedure is similar to that we previously employed in the study of the EFG in other *bixbyites* [29, 57, 58]. Our interest for this modelling of the doped system remains in the actual treatment of the Ta atom as an impurity located at substitutional defect-free cationic sites C and D of the Y_2O_3 *bixbyite* host structure. In particular, the APW+lo method allows us to calculate the EFGs for the Ta atom located at each cationic site, and to

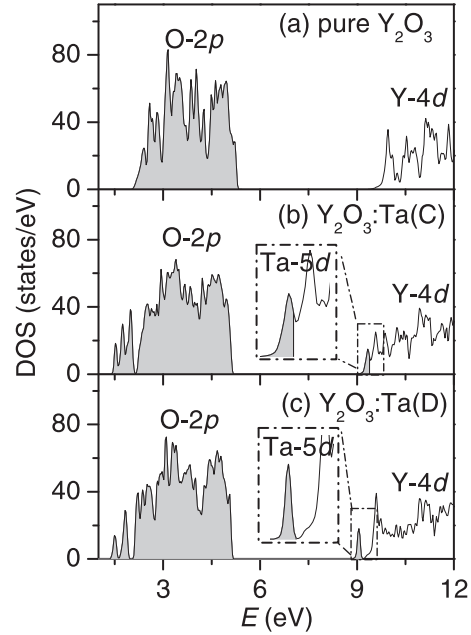


Figure 6. Calculated total DOSs predicted by LDA for (a) pure Y_2O_3 and (b), (c) Ta-doped Y_2O_3 (*relaxed neutral cell*). Shaded areas indicate occupied energy states. In each case, E_{F} is at the end of the shaded area. The magnified sector corresponds to the Ta donor level.

contrast them with the ‘observed’ EFGs by the ^{181}Ta probe in the PAC experiments.

3.2.2. APW+lo results. In figure 6 we present the total DOS for the pure and Ta-doped systems, calculated with the LDA approximation for the relaxed structures. We plot the DOS corresponding to the pristine crystal (figure 6(a)), and we compare it with that of $\text{Y}_2\text{O}_3:\text{Ta}(\text{C})$ and $\text{Y}_2\text{O}_3:\text{Ta}(\text{D})$ (figures 6(b) and (c), respectively). For each DOS, we indicate the most significant orbital contributions. The WCGGA approximation predicts similar DOSs. As can be seen, for pure Y_2O_3 the valence band is dominated by the O-2p states, with a minor admixture of Y-4p and Y-4d orbitals, and the conduction band shows a predominantly Y-4d character, with a smaller contribution of O-2p states. Both bands are separated by a forbidden band gap of about 4.5 eV.

The presence of the Ta atom produces the appearance of impurity donor states near the conduction band bottom, mainly with Ta-5d character. For $\text{Y}_2\text{O}_3:\text{Ta}(\text{C})$, these states are practically located on the conduction band bottom (see the inset in figure 6(b)), while for $\text{Y}_2\text{O}_3:\text{Ta}(\text{D})$ these states form a well-defined deep donor level about 0.5 eV below the conduction band minimum (figure 6(c)).

The simple replacement of a Y atom by a Ta atom (which we called *neutral cell*) produces a system with these donor states completely filled (see shaded areas in figures 6(b) and (c)). As electrons are removed from the cell, the Fermi level (E_{F}) is shifted to lower energies. When two electrons are removed, the donor states become empty, and E_{F} is at the top of the valence band. This result is in agreement with the

Table 1. LDA predictions for the EFGs and the d_{NN} distances from the Ta impurity to its six ONNs, obtained for the different structures and charge states of the cell. Each d_{NN} value has multiplicity of two for site C, and six for site D. In the case of the experimental result, the sign of V_{zz} is not determined.

	Y ₂ O ₃ :Ta(C)		Y ₂ O ₃ :Ta(D)	
	V_{zz} (10^{21} V m ⁻²)	η	d_{NN} (Å)	d_{NN} (Å)
Unrelaxed structure				
Neutral cell	-11.54	0.65		
1e ⁻ removed	-18.90	0.44	2.24, 2.27, 2.33	0 2.28
2e ⁻ removed	-15.13	0.66		0 23.62
Relaxed structure				
Neutral cell	5.72	0.65	1.99, 2.07, 2.16	0 5.03
1e ⁻ removed	-7.65	0.71	1.99, 2.03, 2.15	0 14.71
2e ⁻ removed	-13.71	0.60	1.98, 2.01, 2.11	0 25.94
Experimental result	13.77(6)	0.535(7)		0 24.4(1)

Table 2. LDA predictions for the main *pp*- and *dd*-contributions to the total largest component of the EFG, V_{zz}^{total} (in units of 10^{21} V m^{-2}), obtained for the different relaxed structures and charge states of the cell.

	Y ₂ O ₃ :Ta(C)			Y ₂ O ₃ :Ta(D)		
	V_{zz}^{pp}	V_{zz}^{dd}	V_{zz}^{total}	V_{zz}^{pp}	V_{zz}^{dd}	V_{zz}^{total}
Neutral cell	+17.17	-11.74	+5.72	+30.95	-24.48	+5.03
1e ⁻ removed	-13.56	+7.10	-7.65	+27.60	-12.42	+14.71
2e ⁻ removed	-13.74	-1.21	-13.71	+24.08	+1.23	+25.94

nominal double donor character of Ta⁵⁺ in Y₂³⁺O₃²⁻. In this case, the integration of the atom-projected partial DOS for Ta, Y, and O contributions indicates that only about 0.4 e⁻ of the removed charge is inside the muffin-tin sphere of the Ta atom.

In table 1 we present the EFG results for the different structures and charge states of the Y₂O₃:Ta systems when using LDA. The WCGGA approximation predicts practically the same results. The unrelaxed structure is the same of that of the pure Y₂O₃, wherein the distances d_{NN} from the Ta atom to its six nearest oxygen neighbours (ONN) are equal to those the Y atom has in its own oxide. There are three pairs of d_{NN} values for site C; on the other hand, the value of d_{NN} is the same for the six oxygen atoms at site D. In table 1, we present these d_{NN} values. As can be seen, for the unrelaxed structure there is a strong dependence of V_{zz} with the cell charge state for both sites. For the relaxed structure, the d_{NN} values decrease, being minimum when two electrons are removed from the cell.

We found that the relaxation produces Ta-ONN distances that are in good agreement with those calculated considering the empirical ionic radii [59] and the coordination of Ta and O in the *bixbyite* structure. If we consider the sixfold coordinated Ta atom, and the fourfold coordinated O atom, the summation of their ionic radii gives 2.1 Å for the Ta–O bond-length, which is in the order of magnitude those obtained for the relaxed structures (see table 1). We suppose that the relaxation allows the Ta atom to try a locally reconstruction of the surroundings that it has in its own oxide, TaO₂ (where $d_{\text{NN}} \approx 2.02 \text{ Å}$ [59, 60]). In addition, when we relax the structure, we found that for both sites $|V_{zz}|$ increases with the successive removal of electrons, while η^{C} is kept in the range 0.60–0.71. In particular, we observe that $|V_{zz}^{\text{C}}|$ and $|V_{zz}^{\text{D}}|$, respectively, reach values 240% and 540% higher than those corresponding to the *neutral cell*.

In order to study the origin of the EFG at each impurity site, we decomposed the non-spherical electron density within the Ta atomic sphere according to its orbital symmetries. We found that the total EFGs shown in table 1 are mainly due to the charge inside the Ta sphere. In each case, the V_{zz} main contributions have *p* and *d* character. In table 2 we present these contributions for the relaxed structures. In the case of the *neutral cell*, the *d*-contribution is opposite to the *p* one and of the same order of magnitude. When electrons are removed from the cell, both contributions decrease, but the *d* one decreases faster than the *p* one. For two removed electrons, the *d* contribution is below 10% of the total EFG. Because of this behaviour, the total V_{zz} of the *neutral cell* is the smallest

one, while in the charged cases its value is higher, and with a main contribution of the Ta-5*p* orbitals. These results show that the previously mentioned 0.4 electrons that fill the Ta-5*d* donor states strongly influence the EFG at the impurity site.

3.2.3. Comparison with experiments. If we compare our APW+lo predictions of the EFG with the experimental results, we found an excellent agreement if we consider those calculations corresponding to the relaxed structures with two electrons removed from the cell. According to the considered model, this suggests that experimentally we have the impurity doubly ionized even at room temperature. This result confirms that the cationic sites in which the ¹⁸¹Ta probes are mainly located through the PSG method are free of defects Y₂O₃ crystalline sites.

Finally, we performed additional calculations to understand the experimental $f_{\text{C}}/f_{\text{D}}$ ratio dependence on *T*. To this purpose, we considered from first-principles Hf-doped Y₂O₃ systems, in order to take into account that ¹⁸¹Hf is the isotope parent of the ¹⁸¹Ta PAC probe. We applied the same calculation parameters and convergence criteria as those used for the Ta-doped systems. For the *neutral cell*, using LDA and WCGGA we found that the energy of the Y₂O₃:Hf(D) system is about 0.1 eV smaller than that of the Y₂O₃:Hf(C) system. These results could explain the evolution with the measuring temperature of the $f_{\text{C}}/f_{\text{D}}$, which ranges from 8 to 3.4. If we assume that the radioactive impurity does not jump from one site to the other during the ¹⁸¹Hf → ¹⁸¹Ta decay, as everybody usually assumes, our energy calculation suggests a ¹⁸¹Ta preference for site D. Consequently, despite the initial value $f_{\text{C}}/f_{\text{D}} = 8$ is far from the case of both cationic sites occupied by the probe with equal probability (i.e., $f_{\text{C}}/f_{\text{D}} = 3$), if we consider that increasing temperature promotes ionic exchange in the sample, we could expect the observed shift to smaller values of the $f_{\text{C}}/f_{\text{D}}$ ratio as *T* increases.

4. Conclusions

In this study, we showed that the PSG method followed by a thermal treatment at 1473 K successfully synthesizes pure and ¹⁸¹Ta-doped Y₂O₃ with the cubic *bixbyite* structure. The obtained samples were characterized by different experimental techniques. Among them, the SEM micrographs allowed the comparison of the PSG sample with a commercial Y₂O₃ powder pellet subjected to the same thermal process, and showed that a distinctive feature of the PSG sample is the




presence of micropores. On the other hand, the PAC spectroscopy using ^{181}Ta impurities as probe-atoms showed that the impurity mainly locates at substitutional cationic sites C and D of the *bixbyite* structure. The measured EFGs at both sites are in very good agreement with those previously obtained in a sample prepared by ^{181}Hf ion implantation of the commercial powder. Our experimental results are also consistent with the prediction of the well-established ^{181}Ta EFG systematics for rare-earth *bixbyites* [18, 26]. In addition, our experimental interaction assignment is supported by the APW+lo calculations of the EFG tensor, which confirm that the cationic sites in which the probes are located in both experiments ([25] and this work) are free of defects. When a Ta impurity substitutes the cation of the host structure of this semiconductor oxide, our calculations show that Ta modifies the local structure through a shortening of the distances to its oxygen nearest neighbours. Moreover, it induces the appearance of Ta-5d donor states in the DOS of the doped system. We found that the EFG at the Ta site strongly depends on the degree of occupancy of these donor states, and that the best agreement between theory and experiment happens when we consider these states completely unoccupied. This corresponds to the Ta impurity doubly ionized, in accordance with the double donor character that Ta has in Y_2O_3 , and means that the measured EFGs are mainly due to the Ta-5p charge distribution along the valence band. Calculations also show that the ground state energy for ^{181}Hf ($\rightarrow^{181}\text{Ta}$) occupying D sites is smaller than that for C sites. This site occupancy preference can explain the behaviour of the f_C/f_D fraction site ratio when temperature increases.

In summary, we found that for this studied oxide, the PSG process is a very effective and rapid route to successfully synthesize the PAC doped sample with the impurity located at substitutional defect-free cationic sites of the host structure. Considering this, we are planning to continue using the PSG method to study in depth the structural and hyperfine properties in other doped semiconductors.

Acknowledgments

We wish to acknowledge the Argentinian and Brazilian funding institutions, Consejo Nacional de Investigaciones Científicas y Técnicas (CONICET, under Grants No. PIP0002 and 112-201501-00803CO), Conselho Nacional de Desenvolvimento Científico e Tecnológico (CNPq, grant no. 305046/2013-6), and Fundação de Amparo a Pesquisa do Estado de São Paulo (FAPESP, grant no. 2014/14001-1). This research made use of the computational facilities of the Physics of Impurities in Condensed Matter (PhI) group at IFLP and Departamento de Física (UNLP). DR wishes to thank the personnel at IPEN for their kind hospitality during his stay, and also wishes to thank to Agencia Nacional de Investigación e Innovación (ANII), Uruguay. MR and DR are members of CONICET, Argentina.

ORCID

Diego Richard  <https://orcid.org/0000-0002-0799-7611>
 Mario Rentería  <https://orcid.org/0000-0003-1396-4792>
 Artur Wilson Carbonari  <https://orcid.org/0000-0002-4499-5949>

References

- [1] Dietl T 2010 A 10 year perspective on dilute magnetic semiconductors and oxides *Nat. Mater.* **9** 965–74
- [2] Wang S, An Y, Feng D, Wu Z and Liu J 2013 The local structure, magnetic, and transport properties of Cr-doped In_2O_3 films *J. Appl. Phys.* **113** 153901
- [3] Lamas D G, Bianchetti M F, Cabezas M D and Walsøe de Reca N E 2010 Nanostructures ceramic materials: applications in gas sensors and solid-oxide fuel cells *J. Alloy Compd.* **495** 548–51
- [4] Miller D R, Akbar S A and Morris P A 2014 Nanoscale metal oxide-based heterojunctions for gas sensing: a review *Sensors Actuators B* **204** 250–72
- [5] Kim H J and Lee J H 2014 Highly sensitive and selective gas sensors using p-type oxide semiconductors: overview *Sensors Actuators B* **192** 607–27
- [6] Guan Y, Wang D, Zhou X, Sun P, Wang H, Ma J and Lu G 2014 Hydrothermal preparation and gas sensing properties of Zn-doped SnO_2 hierarchical architectures *Sensors Actuators B* **191** 45–52
- [7] Jing Z, Ling B, Yu Y, Qi W and Zhang S 2015 Preparation and gas sensing activity of La and Y Co-doped titania nanoparticles *J. Sol-Gel Sci. Technol.* **73** 112–7
- [8] Lima M K, Fernandes D M, Silva M F, Baesso M L, Neto A M, de Moraes G R, Nakamura C V, de Oliveira Caleare A, Winkler Hechenleitner A A and Gómez Pineda E A 2014 Co-doped ZnO nanoparticles synthesized by an adapted sol-gel method: effects on the structural, optical, photocatalytic and antibacterial properties *J. Sol-Gel Sci. Technol.* **72** 301–9
- [9] Babić B, Zarubica A, Arsić T M, Pantić J, Jokić B, Abazović N and Matović B 2016 Iron doped anatase for application in photocatalysis *J. Eur. Ceram. Soc.* **36** 2991–6
- [10] Joh D W, Rath M K, Park J W, Park J H, Cho K H, Lee S, Yoon K J, Lee J H and Lee K T 2016 Sintering behavior and electrochemical performances of nano-sized gadolinium-doped ceria via ammonium carbonate assisted co-precipitation for solid oxide fuel cells *J. Alloy Compd.* **682** 188–95
- [11] De la Luz V, Prades M, Beltrán M and Cordoncillo E 2013 Environmental-friendly yellow pigment based on Tb and M (M = Ca or Ba) Co-doped Y_2O_3 *J. Eur. Ceram. Soc.* **33** 3359–68
- [12] Ciciliati M A, Silva M F, Fernandes D M, de Melo M A C, Hechenleitner A A W and Pineda E A G 2015 Fe-doped ZnO nanoparticles: synthesis by a modified sol-gel method and characterization *Mater. Lett.* **159** 84–6
- [13] Liu H, Zhao K, Wang T, Deng J and Zeng H 2015 Facile preparation of cerium (Ce) and antimony (Sb) codoped SnO_2 for hydrogen production in lactic acid solution *Mater. Sci. Semicond. Process.* **40** 670–5
- [14] Sena C, Costa M S, Muñoz E L, Cabrera-Pasca G A, Pereira L F D, Mestnik-Filho J, Carbonari A W and Coaquira J A H 2015 Charge distribution and hyperfine interactions in the vicinity of impurity sites in In_2O_3 doped with Fe, Co, and Ni *J. Magn. Magn. Mater.* **387** 165–78
- [15] Garza-Arévalo J I, García-Montes I, Hinojosa Reyes M, Guzmán-Mar J L, Rodríguez-González V and

- Hinojosa Reyes L 2016 Fe doped TiO₂ photocatalyst for the removal of As(III) under visible radiation and its potential application on the treatment of As-contaminated groundwater *Mater. Res. Bull.* **73** 145–52
- [16] Schatz G and Weidinger A 1996 *Nuclear Condensed Matter Physics: Nuclear Methods and Applications* (Chichester: Wiley)
- [17] Uhrmacher M 2007 Application of perturbed angular correlations to oxides *Physica B* **389** 58–66
- [18] Pasquevich A F and Rentería M 2011 Impurity centers in oxides investigated by γ - γ perturbed angular correlation spectroscopy and *ab initio* calculations *Defect Diffus. Forum* **311** 62–104
- [19] Carbonari A W, Mestnik-Filho J, Attili R N, Moralles M and Saxena R N 1999 Electric field gradient in bixbyite rare-earth oxides R₂O₃ (R = Tl, Eu, Lu, Tm) measured by perturbed angular correlation *Hyperfine Interact.* **120/121** 475–8
- [20] Wolf H, Deubler S, Forkel-Wirth D, Foettinger H, Iwatschenko-Borho M, Meyer F, Renn M, Witthuhn W and Helbig R 1986 Acceptors and donors in the wide-gap semiconductors ZnO and SnO₂ *Mater. Sci. Forum* **10–12** 863–8
- [21] Shitu J, Wiarda D, Wenzel T, Uhrmacher M, Lieb K P, Bedi S and Bartos A 1992 Electric-field gradients in Sm₂O₃, Gd₂O₃, and Ho₂O₃ measured with perturbed-angular-correlation spectroscopy *Phys. Rev. B* **46** 7987–93
- [22] Kessler P, Lorenz K and Vianden R 2011 Implanted impurities in wide band gap semiconductors *Defect Diffus. Forum* **311** 167–79
- [23] Uhrmacher M, Attili R N, Lieb K P, Winzer K and Mekata M 1996 Perturbed angular correlation measurements in 2D spin-frustrated CuFeO₂ *Phys. Rev. Lett.* **76** 4829
- [24] Lupascu D, Habenicht S, Lieb K P, Neubauer M, Uhrmacher M and Wenzel T 1996 Relaxation of electronic defects in pure and doped La₂O₃ observed by perturbed angular correlations *Phys. Rev. B* **54** 871
- [25] Pasquevich A F, Bibiloni A G, Massolo C P, Rentería M and Vercesi J A 1994 Electric-field gradients at the ¹⁸¹Ta impurity site in Yb, Y, and Dy sesquioxides *Phys. Rev. B* **49** 14331–6
- [26] Muñoz E L, Darriba G N, Bibiloni A G, Errico L A and Rentería M 2010 Ionic exchange of Hf donor impurities in the wide-gap semiconductor Tm₂O₃ *J. Alloy Compd.* **495** 532–6
- [27] Richard D, Darriba G N, Muñoz E L, Errico L A and Rentería M 2014 Ionic exchange and the local structure in the HfO₂/Ho₂O₃ system studied by PAC spectroscopy *J. Alloy Compd.* **594** 189–96
- [28] Rentería M, Requejo F G, Bibiloni A G, Pasquevich A F, Shitu J and Freitag K 1997 Perturbed-angular-correlation study of the electric-field gradient in ¹⁸¹Hf-doped and implanted indium sesquioxide *Phys. Rev. B* **55** 14200–7
- [29] Richard D, Darriba G N, Muñoz E L, Errico L A, Eversheim P D and Rentería M 2016 Experimental and first-principles theoretical study of structural and electronic properties in Ta-doped In₂O₃ semiconductor: finding a definitive hyperfine interaction assignment *J. Phys. Chem. C* **120** 5640–50
- [30] Taylor M A, Alonso R E, Errico L A, López-García A, de la Presa P, Svane A and Christensen N E 2010 Coexistence of different charge states in Ta-doped monoclinic HfO₂: theoretical and experimental approaches *Phys. Rev. B* **82** 165203
- [31] Taylor M A, Alonso R E, Errico L A, López-García A, de la Presa P, Svane A and Christensen N E 2012 Structural, electronic, and hyperfine properties of pure and Ta-doped m-ZrO₂ *Phys. Rev. B* **85** 155202
- [32] Pechini M P 1967 *US Patent* US 3330697:6
- [33] Singh A K, Kutty T R G and Sinha S 2012 Pulsed laser deposition of corrosion protective yttrium oxide (Y₂O₃) coating *J. Nucl. Mater.* **420** 374–81
- [34] Hou X, Zhou S, Jia T, Lin H and Teng H 2011 White light emission in Tm³⁺/Er³⁺/Yb³⁺ tri-doped Y₂O₃ transparent ceramic *J. Alloy Compd.* **509** 2793–6
- [35] Mao X, Li X, Feng M, Fan J, Jiang B and Zhang L 2015 Cracks in transparent La-doped yttria ceramics and the formation mechanism *J. Eur. Ceram. Soc.* **35** 3137–43
- [36] Li X, Mao X, Feng M, Qi S, Jiang B and Zhang L 2016 Fabrication of transparent La-doped Y₂O₃ ceramics using different La₂O₃ precursors *J. Eur. Ceram. Soc.* **36** 2549–53
- [37] Fukabori A, Sekita M, Ikegami T, Iyi N, Komatsu T, Kawamura M and Suzuki M 2007 Induced emission cross section of a possible laser line in Nd:Y₂O₃ ceramics at 1.095 μ m *J. Appl. Phys.* **101** 043112
- [38] Maslen N, Streltsov V A and Ishizawa N 1996 A synchrotron x-ray study of the electron density in C-type rare earth oxides *Acta Crystallogr. B* **52** 414–22
- [39] Dupont A, Parent C, Le Garrec B and Heintz J M 2003 Size and morphology control of Y₂O₃ nanopowders via a sol-gel route *J. Solid State Chem.* **171** 152–60
- [40] Chen W, Li F, Liu L and Li Y 2006 Synthesis of nano-sized yttria via a sol-gel process based on hydrated yttrium nitrate and ethylene glycol and its catalytic performance for thermal decomposition of NH₄ClO₄ *J. Rare Earth* **24** 543–8
- [41] Lakshminarasappa B N, Shivaramu N J, Nagabhushana K R and Singh F 2014 Synthesis characterization and luminescence studies of 100 MeV Si⁸⁺ ion irradiated sol gel derived nanocrystalline Y₂O₃ *Nucl. Instrum. Methods B* **329** 40–7
- [42] Hajizadeh-Oghaz M, Shoja Razavi R, Barekat M, Naderi M, Malekzadeh S and Rezazadeh M 2016 Synthesis and characterization of Y₂O₃ nanoparticles by sol-gel process for transparent ceramics applications *J. Sol-Gel Sci. Technol.* **78** 682–91
- [43] Sena C, Costa M S, Cabrera-Pasca G A, Saxena R N and Carbonari A W 2013 TDPAC measurements in pure and Fe-doped In₂O₃ *Hyperfine Interact.* **221** 105–10
- [44] Mercúrio M E, Carbonari A W, Cordeiro M R and Saxena R N 2007 Characterization of ZnO and Zn_{0.95}Co_{0.05}O prepared by sol-gel method using PAC spectroscopy *Hyperfine Interact.* **178** 1–5
- [45] Dogra R, Carbonari A W, Mercúrio M E, Cordeiro M R, Ramos J M and Saxena R N 2010 Search for room temperature ferromagnetism in low-concentration transition metal doped ZnO nanocrystalline powders using a microscopic technique *IEEE Trans. Magn.* **46** 1780–3
- [46] Blaha P, Schwarz K, Madsen G, Kvasnicka D and Luitz J 2012 *WIEN2k: An Augmented Plane Wave+Local Orbitals Program for Calculating Crystal Properties* (Vienna: Vienna University of Technology)
- [47] Valentini R and Vianden R 2010 PAC studies with LSO scintillation crystals *Nucl. Instrum. Methods A* **623** 1002–8
- [48] Larson A C and Von Dreele R B 2004 *General Structure Analysis System (GSAS) Report* LAUR 86:748 Los Alamos National Laboratory
- [49] Durán P, Tartaj J and Moure C 2002 Sintering behaviour of Y₂O₃ powders prepared by the polymer complex solution method *Ceram. Int.* **28** 791–803
- [50] Dupont A, Largeteau A, Parent C, Le Garrec B and Heintz J M 2005 Influence of the yttria powder morphology on its densification ability *J. Eur. Ceram. Soc.* **25** 2097–103
- [51] Stone N J 2005 Table of nuclear magnetic dipole and electric quadrupole moments *Atom. Data Nucl. Data* **90** 75–176
- [52] Errico L A, Rentería M, Bibiloni A G and Freitag K 2007 Electric-field gradients at ¹⁸¹Ta impurity sites in Ho₂O₃ and Eu₂O₃ bixbyites *Physica B* **389** 124–9

- [53] Perdew J P and Wang Y 1992 Accurate and simple analytic representation of the electron-gas correlation energy *Phys. Rev. B* **45** 13244–9
- [54] Wu Z and Cohen R E 2006 More accurate generalized gradient approximation for solids *Phys. Rev. B* **73** 235116
- [55] Blaha P, Schwarz K and Dederichs P H 1988 First-principles calculation of the electric-field gradient in hcp metals *Phys. Rev. B* **37** 2792–6
- [56] Schwarz K, Ambrosch-Draxl C and Blaha P 1990 Charge distribution and electric-field gradients in $\text{YBa}_2\text{Cu}_3\text{O}_{7-x}$ *Phys. Rev. B* **42** 2051–61
- [57] Richard D, Muñoz E L, Errico L A and Rentería M 2012 Electric-field gradients at Ta impurities in Sc_2O_3 semiconductor *Physica B* **407** 3134–6
- [58] Richard D, Muñoz E L, Rentería M, Errico L A, Svane A and Christensen N E 2013 *Ab initio* LSDA and LSDA+U study of pure and Cd-doped cubic lanthanide sesquioxides *Phys. Rev. B* **88** 165206
- [59] Shannon R D 1976 Revised effective ionic radii and systematics studies in interatomic distances in alides and chalcogenides *Acta Crystallogr. A* **32** 751–67
- [60] Schönberg N 1954 An x-ray Investigation of the tantalum–oxygen system *Acta Chem. Scand.* **8** 240–5